Morpholine sulfur trifluoride: Vibrational spectra, conformational properties and crystal structure

Andrea Flores Antognini [a], Norma L. Robles [a,*], Edgardo H. Cutin [a,*], Eduard Bernhardt [b], Markus Hirschberg [b], Xiaoqing Zeng [b], Helge Willner [b], Heinz Oberhammer [c]

[a] INQUINOA (CONICET-UNT) Instituto de Química Física, Facultad de Bioquímica, Química y Farmacia, Universidad Nacional de Tucumán, San Lorenzo 456, (4000) Tucumán, Argentina
[b] FB C, Anorganische Chemie, Bergische Universität Wuppertal, Gaußstrasse 20, 42119 Wuppertal, Germany
[c] Institut für Physikalische und Theoretische Chemie, Universität Tübingen, 72076 Tübingen, Germany

A B S T R A C T

Analysis of the vibrational spectra and quantum chemical calculations for morpholine sulfur trifluoride, $SF_3N(CH_2CH_2)_2O$, demonstrate that the morpholine ring possesses chair conformation and occupies an equatorial position of the trigonal bipyramidal SF$_3$ group. The compound exists in the gas phase as a mixture of two conformers. The conformer with the SF$_3$ group in equatorial orientation relative to the six-membered morpholine ring is slightly more stable than the axial conformer and the equilibrium is surprisingly temperature independent. MP2 and B3LYP calculations with cc-pVTZ basis sets predict free energy differences $\Delta G^\circ = G^\circ_{ax} - G^\circ_{eq}$ of +0.18 and +0.40 kcal/mol, respectively. At temperatures below 12 °C the title compound crystallizes and the structure of the equatorial conformer, which is the only form present in the crystal, was determined by X-ray diffraction. At 131(1) K a phase transition occurs and the low and high temperature forms were studied at 100 and 150 K, respectively.

© 2012 Elsevier B.V. All rights reserved.

1. Introduction

The study of the chemistry of sulfur–nitrogen compounds containing single, double or triple sulfur–nitrogen bonds started in the 1950s in account of their peculiar structural and conformational properties as well as due to the interesting nature of these bonds.

The stability of compounds possessing N–S bonds depends strongly on the oxidation state of the sulfur atom. In fact, so far the only reported compound with a single N–S bond and S(+2) is CF$_3$–S–NF$_2$ [1], whereas several S(+6)-compounds such N≡SF$_2$–N=SF$_2$ and N≡SF$_2$–N=S(O)F$_2$, possessing not only a single, but also a triple sulfur–nitrogen bond, have recently been prepared and characterized [2]. In contrast, plenty stable S(+4) compounds with N=S double bond have been studied so far, for example molecules of the type R–N=SX$_2$ (CF$_3$N=SF$_2$ [3], CF$_3$N=SCl$_2$ [4], FC(O)N=SF$_2$ [5], FC(O)N=SCl$_2$ [6], C$_2$F$_5$N=SF$_2$ [7], C$_2$F$_5$N=SCl$_2$ [8] and CH$_3$N=S(CF$_3$)$_2$ [9]) and RN=S=O (CF$_3$–N=S=O and SF$_5$N=S=O [10]). However, those which have attracted our present interest are the S(+4)-compounds with single N–S bonds, particularly a substance containing the entity N–SF$_3$, in account of its influence on the reactivity and the conformational properties.

(C$_2$H$_5$)$_2$N–SF$_3$ is known as DAST (diethyl aminosulfur trifluoride) and has vastly proved to be a useful fluorinating agent [11]. However, it has the potential to decompose violently when heated and presents a hazard if not handled properly [12]. In account of its higher thermal stability and its better efficiency, morph-SF$_3$ (morpholine sulfur trifluoride, see Fig. 1) was preferred to achieve the transformation of alcohols to alkyl fluorides and of ketones to gem-difluorides [12–14], for example. This heterocycle must exhibit peculiar conformational behavior, which makes it more appropriate to accomplish these reactions.

In a series of N-substituted morpholine molecules, the barriers to ring inversion change due to the conjugative effects of substituents on the nitrogen atom, which strengthen the double bond character between nitrogen and its vicinal atom [15] (see Scheme 1). It has been found that the rotational barrier increases and the ring inversion barrier decreases with the increment of the double bond character. This fact is attributed to the double bond character in the exocyclic bond. Shortly, the substitution at the nitrogen atom determines a definite conformational preference of the ring.

Morpholine sulfur trifluoride is a commercial product and widely used, but it is still insufficiently characterized. Here we present its thermal, spectroscopic and structural properties. The possible conformers will be studied by infrared spectra of samples held at different temperatures before matrix isolation. These results are complemented by X-ray crystallography, Raman spectra of the solid, and quantum chemical calculations at different
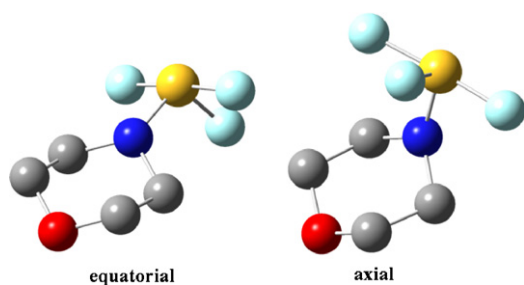
Fig. 1. Schematic representation of SF$_3$N(CH$_2$CH$_2$)$_2$O, morph-SF$_3$.
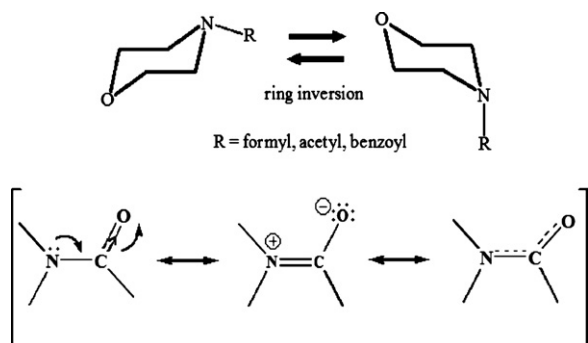
Scheme 1. Conformational possibilities of some N-substituted morpholine molecules.

levels of theory. It is expected that this analysis will allow us to understand the structural, conformational and vibrational properties of this interesting molecule in relation to the identity of the substituent at the nitrogen atom.

2. Materials and methods

2.1. Properties of the morph-SF$_3$ sample

Liquid morph-SF$_3$ is a commercial product (ABCR, Karlsruhe), which hydrolyses easily and must be handled in a dry box. The purchased sample was thoroughly degassed and the melting point observed at 12 °C, and the vapor pressure measured to be 0.25 mbar at room temperature.

We realized that morph-SF$_3$ is little characterized and to the best of our knowledge ^{19}F NMR (ether): δ = 56.74 (d, $J_{F–F}$ = 55 Hz, 2F), 18.08 (t, $J_{F–F}$ = 55 Hz, 1F) ppm are the only published spectroscopic data [16].

^{1}H, ^{13}C, and ^{19}F NMR spectra of a neat sample in 4 mm FEP inliners, placed in 5 mm precision glass NMR tube (Wilmad 507 or 528 PPT) have been recorded at 24 °C on a Bruker Avance III spectrometer using external CD$_2$Cl$_2$ lock and operating at 400.17, 100.61 and 376.54 MHz, respectively. The ^{1}H and ^{13}C NMR chemical shifts were referenced with respect to the chemical shifts for CH$_2$Cl$_2$ of 5.32 and 53.5 ppm, respectively. The ^{19}F NMR spectra were referenced externally to a neat CFCl$_3$ sample at 24 °C. δ ^{1}H = 3.85 (m), δ ^{13}C = 67.3 (t, $J_{C–H}$ = 145.3 Hz), 48.2 (t, $J_{C–H}$ = 145.8 Hz), δ ^{19}F = 52.3 (2F), 17.2 (1F) ppm (no coupling resolved). Less than 2% of impurities could be detected in the NMR spectra.

2.2. Vibrational spectroscopy

Raman spectra of morph-SF$_3$ at low temperatures were recorded on a Bruker-Equinox 55 FRA 106/S FT-Raman

spectrometer using a 1064-nm Nd:YAG laser (200 mW) with 64 scans at a resolution of 2 cm^{-1}. A small sample (ca. 20 mg) was condensed in high vacuum onto a stainless steel finger cooled with liquid nitrogen. Subsequently the cold finger was rotated under high vacuum towards the laser beam.

Gas-phase FT-IR spectra in the range 4000–400 cm^{-1} were measured with a resolution of 2 cm^{-1} and 32 scans co-added for each spectrum. The IR gas cell (20 cm optical path length and 0.6 cm thick Si windows) was connected with the vacuum line and contained in the sample compartment of a Bruker Vector 22 FT-IR spectrometer. For conditioning the inner surface, the gas cell was flushed with the vapor of morph-SF$_3$ several times until it does not hydrolyze any more.

Matrix IR spectra were recorded on a FT-IR spectrometer (IFS 66v/S Bruker) in reflectance mode using a transfer optic. A KBr beam splitter and an MCT detector were used in the region of 4000–550 cm^{-1}. For each spectrum, 200 scans at a resolution of 0.5 cm^{-1} were co-added. A few mg of morph-SF$_3$ was placed into a small U trap that was mounted in front of the matrix support and cooled to −30 °C. A stream of argon gas (ca. 2 mmol/h) was passed over the cold sample and the resulting mixtures of morph-SF$_3$ and argon (estimated 1:1000) were forced through a quartz tube (4 mm i.d. with 1 mm pin hole pointing to the matrix support), that was electrically heated at the end over a length of 15 mm. The nozzle was held at 20, 105 and 215 °C, prior deposition of the gas mixture onto the matrix support (a rhodium-plated copper mirror cooled at 15 K by a He continuous flow cryostat). Details of the matrix apparatus has been described elsewhere [17].

2.3. X-ray crystal structure determination

2.3.1. Crystal growth and crystal mounting

In a dry box a small amount (ca. 50 mg) of morph-SF$_3$ was transferred into the upper part of a dry glass container (o.d. 1 cm and length 15 cm), equipped with a valve with a PTFE stem (Young). After evacuation, the lower part of the container (ca. 10 cm) was immersed in an ice/water bath for two days. Colorless crystals were obtained at the bottom of the container. Subsequently the container was cooled with dry ice, filled with 1 atm. of argon, scratched and opened. In a cold N$_2$ gas stream of −40 °C the crystals were quickly poured into a trough. Suitable crystals were selected under the microscope and mounted as previously described [18].

2.3.2. Collection and reduction of X-ray data

Crystals were mounted on an Oxford Diffraction Gemini E Ultra diffractometer, equipped with a 2 K × 2 K EOS CCD area detector, a four-circle κ goniometer, an Oxford Instruments cryojet, and sealed-tube Enhanced (Mo) and Enhanced Ultra (Cu) sources. For data collection, the Mo Kα radiation (λ = 0.71073 Å) was used. The diffractometer was controlled by *CrysAlisPro* Graphical User Interface software [19]. The diffraction data collection strategy was optimized with respect to complete coverage and consisted of 10ω scans with a width of 1°, respectively. The data collection for morph-SF$_3$ was carried out at 100 K and 150 K, in a 1024 × 1024 pixel mode using 2 × 2 pixel binning. Processing of the raw data, scaling of the diffraction data, and application of an empirical absorption correction was completed by using the *CrysAlisPro* program [19].

2.3.3. Solution and refinement of the structure

The solution of the structure was performed by direct methods, which located the positions of all atoms. The final refinement was obtained by introducing anisotropic thermal parameters and the recommended weightings for all atoms. All calculations were

performed using the *WinGX v1.64.05* package program for structure determination, solution refinement, and molecular graphics [20–22].

2.4. Computational details

All the quantum chemical calculations were performed using the GAUSSIAN03 program [23]. Geometry optimizations were performed with the B3LYP [24] and MP2 [25] approximations using 6-311G(d) and cc-pVTZ basis sets and standard gradient techniques with simultaneous relaxation of all the geometric parameters. Natural population analysis and second-order donor–acceptor interaction energies were estimated by using the NBO [26] analysis as implemented in the GAUSSIAN03 program.

3. Results and discussion

3.1. Quantum chemical calculations

In addition to the structural and vibrational properties of morph-SF_3 the conformational properties are of great interest. Several conformations of this compound can occur, depending on the position of the morpholine ring in the trigonal bipyramidal SF_3 group (equatorial or axial), on the structure of the six-membered ring (chair or boat) and on the orientation of the SF_3 group relative to the ring (equatorial or axial). Preliminary low level calculations (HF/6-31G(d)) confirm the usual assumption that the morpholine ring lies in the equatorial plane of the SF_3 group and prefers the chair conformation. The structure with the ring in axial position of the SF_3 group is predicted to be 16.9 kcal/mol higher in energy than

Table 1

Observed and calculated vibrational frequencies (cm^{-1}) and tentative assignment of the 48 fundamental vibrational modes for morpholine sulfur trifluoride.

IR[a]		Raman[a]	Calculated[b]		Approx. desc. [d]
Gas (298 K)	Ar matrix (16 K)[c]	Solid (243 K)	Equatorial (I_{IR})[I_{Raman}]	Axial (I_{IR})[I_{Raman}]	
			3223 (1)[23]	3227 (1)[16]	$\nu_1 CH_2$asym
	3036.6w, br	3033m	3205 (1)[31]	3225 (<1)[59]	$\nu_2 CH_2$asym
2981m	2977.7m	2994s	3157 (4)[84]	3154 (6)[100]	$\nu_3 CH_2$asym
2978m	2971.0m		3155 (6)[55]	3151 (6)[94]	$\nu_4 CH_2$asym
2933w	2931.3m	2936m/2953m, sh	3084 (5)[36]	3104 (7)[86]	$\nu_5 CH_2$ sym
2911w, sh	2905.5w	2903w, br	3070 (7)[31]	3097 (4)[41]	$\nu_6 CH_2$ sym
2869m	2871.5m	2868s	3041 (9)[100]	3057 (6)[86]	$\nu_7 CH_2$ sym
			3038 (8)[42]	3050 (6)[66]	$\nu_8 CH_2$ sym
			1511 (<1)[2]	1512 (1)[3]	$\delta_9 CH_2$ sciss
1462w	1454.9m	1468m	1502 (6)[<1]	1500 (<1)[6]	$\delta_{10} CH_2$ sciss
		1450s	1495 (<1)[3]	1498 (5)[2]	$\delta_{11} CH_2$ sciss
			1491 (<1)[6]	1483 (1)[6]	$\delta_{12} CH_2$ sciss
	1387.8w	1394vw	1432 (1)[1]	1426 (1)[3]	$\delta_{13} CH_2$wagg
1360m	1364.9w	1362vw	1400 (2)[<1]	1399 (3)[2]	$\delta_{14} CH_2$wagg
			1396 (1)[<1]	1391 (3)[1]	$\delta_{15} CH_2$wagg
	1338.6w	1324m	1363 (<1)[<1]	1376 (4)[6]	$\delta_{16} CH_2$wagg
1300w	1297.8w	1300m	1357 (<1)[5]	1361 (1)[<1]	$\delta_{17} CH_2$twist
1265m, sh	1269.4s/1264.2m		1337 (3)[2]	1333 (4)[4]	$\delta_{18} CH_2$twist
1238s	1230.9m		1303 (10)[<1]	1298 (9)[<1]	$\delta_{19} CH_2$twist
		1219m	1250 (<1)[4]	1252 (<1)[4]	$\delta_{20} CH_2$twist
		1148w	1203 (<1)[<1]	1190 (6)[<1]	ν_{21}C–O
1129s	1132.4vs	1131w	1180 (25)[<1]	1173 (21)[1]	ν_{22}C–O
1129sh	1122.7s	1119vw	1155 (21)[2]	1160 (9)[2]	ν_{23}C–N
1077m	1082.6m	1082m	1115 (11)[4]	1099 (9)[7]	ν_{24}C–C
	1071.2m		1098 (2)[<1]	1090 (4)[<1]	ν_{25}C–N
	1023.1m	1016m	1053 (1)[2]	1045 (4)[3]	ν_{26}C–C
966s	966.6vs	958w	1002 (45)[1]	1000 (42)[2]	ν_{27}N–S
949m			961 (7)[<1]	935 (4)[<1]	$\rho_{28} CH_2$
	859.2vw	865m	889 (<1)[2]	870 (<1)[5]	$\rho_{29} CH_2$
		852m, sh	870 (<1)[<1]	860 (<1)[2]	$\rho_{30} CH_2$
772w, br	766.8s/754.0m	740s	784 (37)[8]	764 (35)[10]	ν_{31}S–F$_{eq}$
657m, sh	696.6m	698m	712 (11)[4]	710 (12)[6]	$\rho_{32} CH_2$
645vs	623.4vs, br	609m	688 (100)[<1]	687 (100)[1]	ν_{33}S–F$_{ax}$
599w, br	593.2vw	576w	615 (2)[1]	596 (4)[1]	δ_{34} ring def.
		509w	533 (1)[2]	527 (<1)[3]	ζ_{35} ring def.
		490m	507 (11)[4]	506 (6)[1]	ν_{36}S–F$_{ax}$
		480w, sh	476 (<1)[<1]	497 (4)[3]	δ_{37}
			467 (3)[<1]	469 (5)[2]	δ_{38}
		431m	428 (1)[<1]	441 (3)[1]	δ_{39}
		383m	393 (3)[1]	414 (3)[<1]	δ_{40}
		362m	365 (1)[1]	404 (2)[<1]	δ_{41}
		294m	330 (2)[1]	345 (2)[<1]	δ_{42}
		275w, sh	296 (<1)[1]	330 (<1)[2]	δ_{43}
			284 (3)[<1]	315 (2)[1]	δ_{44}
		244w	241 (1)[<1]	207 (1)[1]	δ_{45}
		182w	177 (1)[<1]	187 (1)[<1]	δ_{46}
		85vs	80 (<1)[<1]	85 (<1)[1]	δ_{47}
			54 (<1)[<1]	41 (<1)[<1]	τ_{48}

[a] Experimental band positions and relative intensities: vs: very strong, s: strong, m: medium strong, w: weak, vw: very weak, br: broad, and sh: shoulder, ax: axial, eq: equatorial, asym: asymmetric, sym: symmetric, sciss: scissoring, wagg: wagging, twist: twisting, def: deformation.

[b] MP2/cc-pVTZ level of theory; IR intensities ($km\,mol^{-1}$) in parentheses and Raman intensities ($Å^4\,amu^{-1}$) in square brackets.

[c] Only the band positions of the most intense matrix sites are given.

[d] Assignments were made according to the calculated vibrational displacement vectors of the equatorial conformer.

Table 2
Crystallographic and refinement data for $SF_3N(CH_2CH_2)_2O$, morph-SF$_3$.

Identification code	exp_2248	exp_2249
Temperature	150 K	100 K
Empirical formula	$C_4H_8F_3NOS$	$C_4H_8F_3NOS$
Formula weight	175.17	175.17
Wavelength	0.71073 Å	0.71073 Å
Crystal system, space group	Monoclinic, $P2_1/n$ (No. 14)	Monoclinic, $P2_1/c$ (No. 14)
Unit cell dimensions	$a = 6.6703(4)$ Å	$a = 13.3503(6)$ Å
	$b = 7.9740(5)$ Å	$b = 7.9113(2)$ Å
	$c = 12.8918(9)$ Å	$c = 14.2747(8)$ Å
	$\beta = 90.340(6)°$	$\beta = 116.628(6)°$
Volume (Å^3)	685.69(7)	1347.76(10)
Z (molecules per unit cell)	4	8
Calculated density (mg/m^3)	1.697	1.727
Absorption coefficient (mm^{-1})	0.461	0.469
Absorption correction	Analytical	Analytical
Crystal size	$0.28 \times 0.32 \times 0.52$ mm	$0.28 \times 0.32 \times 0.52$ mm
Reflections collected/unique/observed	3315/1590/1389	11309/3251/2847
R_{int}	0.0205	0.0243
R_σ	0.0288	0.0226
Completeness to $\theta = 26.40°$ (0.8 Å)	99.9%	99.9%
Data/restraints/parameters	1590/0/91	3251/0/181
Goodness-of-fit on F^2	1.048	1.090
R indices [$I > 2\sigma(I)$]	$R1 = 0.0339$, $wR2 = 0.0785$	$R1 = 0.0291$, $wR2 = 0.0702$
R indices (all data)	$R1 = 0.0411$, $wR2 = 0.0835$	$R1 = 0.0360$, $wR2 = 0.0743$
Largest diff. peak and hole	0.301 and -0.252 e Å^{-3}	0.417 and -0.336 e Å^{-3}

that with the ring in equatorial position and the boat structure of the ring is predicted to be 9.3 kcal/mol higher than the chair conformation. DFT-B3LYP and MP2 calculations with small (6-31G(d)) and large basis sets (cc-pVTZ) were performed only for the two conformers differing in the orientation (equatorial or axial) of the SF$_3$ group relative to the morpholine ring (see Fig. 1). The two local minima for equatorial and axial orientation were confirmed by the absence of imaginary frequencies. These two conformers differ not only by the orientation of the SF$_3$ group relative to the morpholine ring, but also by the orientation of the S–F$_{eq}$ bond of the SF$_3$ group. In the equatorial conformer this bond points away from the ring and in the axial conformer it points towards the ring. In both conformers the S–F$_{eq}$ bond is located *anti* to the nitrogen lone pair (lp(N)) and strong orbital interactions lp(N) → σ*(S–F$_{eq}$) (anomeric effects) stabilize these orientations. The free energy differences $\Delta G° = G°_{ax} - G°_{eq}$ predicted by the four computational methods are rather similar and small:

$\Delta G°_{298}$ = +0.41 kcal/mol (B3LYP(6-31G(d)), +0.40 kcal/mol (B3LYP/cc-pVTZ), −0.17 kcal/mol (MP2/6-31G(d)) and +0.18 kcal/mol (MP2/ccpVTZ). This small energy difference is surprising, since usually axial conformers are less favored due to higher steric interactions which in this compound are compensated by different strengths of the anomeric effects. According to NBO analyses this anomeric effect lp(N) → σ*(S–F$_{eq}$) is considerably stronger in the axial form (22 kcal/mol) than in the equatorial form (17 kcal/mol). According to the calculated $\Delta G°_{298}$ values a mixture of both conformers with similar concentrations (equatorial form between 67% and 43%) is predicted. Calculated vibrational frequencies are included in Table 1 and structural parameters of the equatorial conformer are listed together with the crystal data in Table 3 (vide infra).

3.2. Vibrational spectroscopy

Most of the $3N - 6 = 48$ fundamental vibrational modes expected for the morpholine sulfur trifluoride molecule were observed in the spectra depicted in Fig. 2. In Table 1 the IR band positions and estimated band intensities of a gaseous and of an argon matrix isolated sample (ca 1:1000) are listed together with a tentative assignment based on the calculated displacement vectors. The Raman frequencies observed of a solid sample at 243 K were included in Table 1 as well. Frequencies of the fundamentals and their intensities were obtained at the MP2/cc-pVTZ level of theory for the equatorial and axial conformers of the title molecule for comparison purposes. In general the calculated band positions and intensities are in good agreement with the recorded spectra.

Matrix IR spectra and their dependence on the temperature of the gas before deposition have been shown to be a very powerful tool to determine conformational properties of gaseous samples [27–29]. This method is based on small differences in vibrational frequencies of the conformers, which are resolved in matrix spectra, on their relative intensities and their variation with temperature. In the case of morph-SF$_3$, however, quantum chemical calculations (B3LYP and MP2 with cc-pVTZ basis sets) predict for almost all strong IR bands differences of less than 3 cm^{-1}. The only strong IR vibration with a large predicted shift of 20 cm^{-1} (MP2) or 12 cm^{-1} (B3LYP) is the S–F$_{eq}$ stretch at
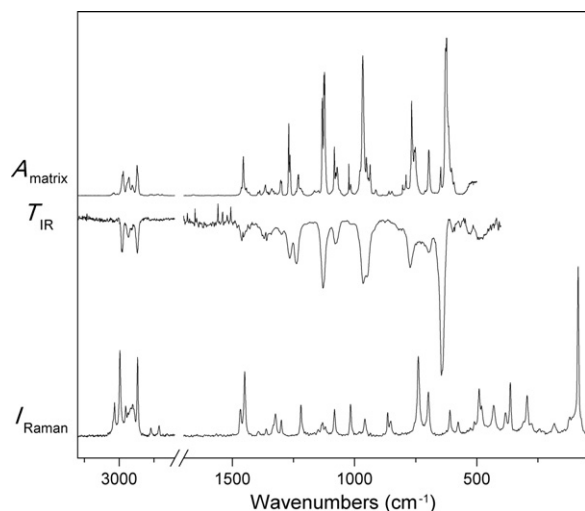

Fig. 2. Upper trace IR spectrum of morph-SF$_3$ isolated in an argon matrix at 15 K (absorbance A, resolution 0.5 cm^{-1}). Middle trace IR spectrum of gaseous morph-SF$_3$ at 298 K (transmision T, resolution 2 cm^{-1}). Lower trace Raman spectrum of solid morph-SF$_3$ at 243 K (Raman intensity I, resolution 2 cm^{-1}).
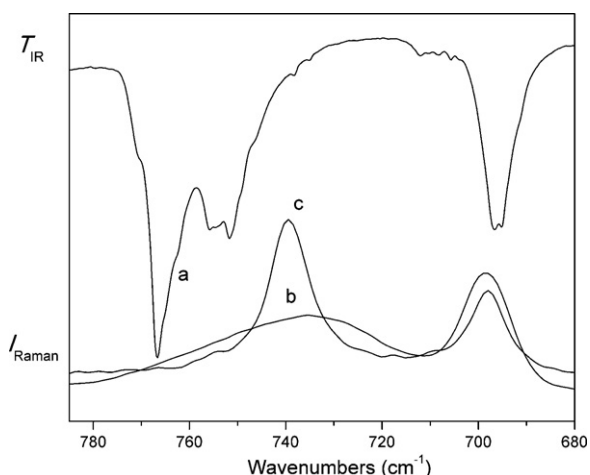
Fig. 3. Trace a: part of the Ar-matrix IR spectrum of morph-SF$_3$. The bands at 766.8/754.0 cm^{-1} are attributed to the equatorial and axial conformers, respectively. Trace b: Raman spectra of amorphous solid at 77 K and trace c: crystalline solid at 243 K in the range of 785–680 cm^{-1}.

766.8/754.0 cm^{-1}. This pair of Ar matrix bands is shown in Fig. 3 in expanded scale and is compared with the Raman spectrum of the amorphous solid at 77 K and the annealed solid at 243 K. This shift between the two conformers can be explained by the different strength of the anomeric effects (see above). The stronger orbital interaction in the axial conformer (22 kcal/mol) leads to an increased weakening of this bond and thus to a lower frequency of the stretching vibration.

In an additional experiment, the morph-SF$_3$/Ar gas mixture passed the spray-on-nozzle at room temperature, 105, or at 215 °C prior to deposition of the mixture at 15 K. Since similar concentrations of both conformers are present at room temperature, only small changes are expected to occur at higher temperature. Indeed there was a little increase in the relative band intensities I(at 754.0)/I(at 766.8 cm^{-1}) with increasing temperature.

Evidence for intermolecular interactions of solid morph-SF$_3$ comes from the temperature dependent Raman spectrum (Fig. S1). During deposition of gaseous morph-SF$_3$ at 77 K in high vacuum, different orientations between O···SF$_3$ of different molecules are retained. Therefore all bands where the SF$_3$ group is involved are broader than the other. During annealing the amorphous solid re-crystallizes and all molecules are equally oriented (see crystal structure).

3.3. Single-crystal X-ray diffraction

X-ray diffraction data of crystalline morph-SF$_3$ were measured at low temperatures and a phase transition at 131(1) K
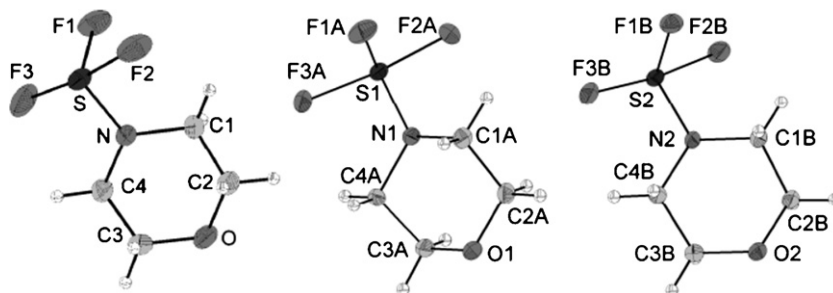
Table 3
Selected bond lengths [Å] and angles [°] for SF$_3$N(CH$_2$CH$_2$)$_2$O.

	exp._2248[b]	exp._2249 (1,a)[b]	exp._2249 (2,b)[b]	MP2/ cc-pVTZ
Bond lengths				
S–N	1.6121(14)	1.6169(12)	1.6143(12)	1.646
S–F(1)	1.5847(12)	1.5947(10)	1.5914(9)	1.601
S–F(2)	1.6727(12)	1.6922(9)	1.6734(9)	1.692
S–F(3)	1.7362(13)	1.7269(10)	1.7680(10)	1.710
N–C(1)	1.483(2)	1.4796(18)	1.4768(18)	1.474
N–C(4)	1.474(2)	1.4832(17)	1.4778(17)	1.471
C(1)–C(2)	1.515(2)	1.516(2)	1.514(2)	1.517
C(3)–C(4)	1.510(2)	1.513(2)	1.5130(19)	1.515
C(2)–O	1.417(2)	1.4217(17)	1.4238(17)	1.415
O–C(3)	1.420(2)	1.4220(18)	1.4232(17)	1.415
S···O	2.9660(12)	3.0018(11)	2.9074(10)	–
Angles				
N–S–F(1)	106.75(7)	105.99(6)	105.94(6)	106.1
N–S–F(2)	91.19(7)	90.79(6)	91.32(5)	89.9
N–S–F(3)	93.05(7)	93.20(5)	93.07(5)	92.1
F(1)–S–F(2)	85.49(7)	85.66(5)	86.10(5)	86.6
F(1)–S–F(3)	85.34(8)	85.95(6)	85.06(5)	86.9
F(2)–S–F(3)	170.68(8)	171.42(6)	170.93(5)	173.5
C(4)–N–C(1)	111.58(13)	111.94(11)	111.68(11)	110.6
C(1)–N–S	123.33(11)	123.09(10)	122.46(9)	120.4
C(4)–N–S	121.27(11)	120.85(9)	120.71(9)	120.0
F(1)–S–N–C(1)	46.63(16)	47.37(13)	43.08(13)	47.5
F(1)–S–N–C(4)	109.48(14)	107.95(11)	109.44(11)	98.5
F(1)–S–N–C(av)	78.06(15)	77.66(12)	76.26(12)	73.0
Δ F(1)–S–N–C[a]	31.43(15)	30.29(12)	33.18(12)	25.5

[a] Torsional angle of the SF$_3$ group away from orientation with C_S symmetry.
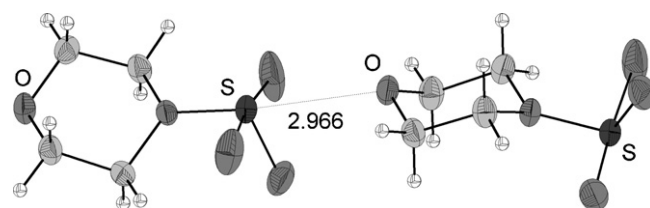[b] Data available as Supporting Information.

Fig. 5. Chainlike linked SF$_3$N(CH$_2$CH$_2$)$_2$O molecules at 150 K (with 50% thermal ellipsoids) by weak intermolecular S···O interactions.

was detected. One and two independent formula units in the unit cells were observed and studied at 150 K, and at 100 K, respectively (Fig. 4).

The crystallographic data for both solid phases are listed in Table 2. During the phase transition only minor changes in the bonding parameters are observed, but at 100 K the cell is doubled (Figs. 5 and 6, Table 3) and the S···O interactions become slightly asymmetric.

The sulfur atom is trigonal bipyramidal coordinated (3F, 1N, 1 electron pair). The S–N bond is orientated relative to the
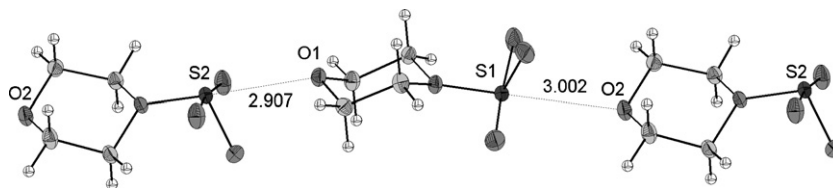

Fig. 4. Molecular structures of the asymmetric unit of SF$_3$N(CH$_2$CH$_2$)$_2$O in the unit cell at 150 K (S, left) and 100 K (S1, S2, right) (with 50% thermal ellipsoids).

Fig. 6. Chainlike linked $SF_3N(CH_2CH_2)_2O$ molecules at 100 K (with 50% thermal ellipsoids) by weak intermolecular S···O interactions.

$N(CH_2CH_2)_2O$ ring in equatorial position and $N(CH_2CH_2)_2O$ is coordinated at SF_3 in the equatorial position as well. The interatomic distances and angles observed for morph-SF_3 are in the typical range (Table 3) and in good agreement with the calculated data. The most prominent deviations are found for the torsional angle Δ (F(1)–S–N–C) out of C_s symmetry, due to intermolecular interactions and packing effects. Both solid phases are stabilized by intermolecular bonds of the types S···O (Figs. 5 and 6). These build in both structures a one dimensional S···O bonds network.

4. Conclusions

Morpholine sulfur trifluoride present several different conformations depending on the position of the morpholine ring in the trigonal bipyramidal SF_3 group, on the structure of the six-membered ring and on the orientation of the SF_3 group relative to the ring. Theoretical calculations confirm the usual assumption that the morpholine ring lies in the equatorial plane of the SF_3 group and prefers the chair conformation, being the equatorial disposition of the SF_3 the most favorable structure in energy terms. This may be rationalized taking into account the strength of several anomeric interactions. The predicted conformational equilibrium between equatorial and axial forms was only discernible in a few signals of the IR Ar matrix spectra, and it is surprisingly temperature independent. No evidence of an additional conformer was found by X-ray crystallography.

Supplementary data

Raman spectra of solid morph-SF_3 at different temperatures. The crystallographic data for the structures in this paper have been deposited with the Cambridge Crystallographic Data Center as supplementary publication nos. CCDC 883291 and 883292. Copies of the data can be obtained free of charge, on application to CCDC, 12 Union Road, Cambridge CB2 1EZ, UK (Fax: +44 1223 336033 or deposit@ccdc.cam.ac.uk).

Appendix A. Supplementary data

Supplementary data associated with this article can be found, in the online version, at http://dx.doi.org/10.1016/j.jfluchem.2012.07.003.

References

[1] O. Glemser, R. Mews, Advances in Inorganic Chemistry 14 (1972) 333–390.
[2] A. Flores Antognini, N.L. Robles, E.H. Cutin, H. Oberhammer, Journal of Molecular Structure 976 (2010) 3–10.
[3] N.L. Robles, E.H. Cutin, C.O. Della Védova, Journal of Molecular Structure 784 (2006) 265–268.
[4] R.M.S. Álvarez, E.H. Cutin, R.M. Romano, C.O. Della Védova, Spectrochimica Acta, Part A 55 (1999) 2615–2622.
[5] R.M.S. Álvarez, E.H. Cutin, R.M. Romano, C.O. Della Védova, Spectrochimica Acta, Part A 52 (1996) 667–673.
[6] C. Leibold, R.M.S. Álvarez, E.H. Cutin, C.O. Della Vedova, H. Oberhammer, Inorganic Chemistry 42 (2003) 4071–4075.
[7] N.L. Robles, E.H. Cutin, R. Mews, C.O. Della Védova, Journal of Molecular Structure 978 (2010) 131–135.
[8] N.L. Robles, R.M.S. Álvarez, E.H. Cutin, C.O. Della Védova, M.F. Erben, R. Boese, H. Willner, R. Mews, European Journal of Inorganic Chemistry 22 (2007) 3535–3542.
[9] F. Trautner, R.M.S. Álvarez, E.H. Cutin, N.L. Robles, R. Mews, H. Oberhammer, Inorganic Chemistry 44 (2005) 7590–7594.
[10] A. Flores Antognini, H. Oberhammer, E.H. Cutin, N.L. Robles, Journal of Molecular Structure (2012), http://dx.doi.org/10.1016/j.molstruc.2012.04.016.
[11] M. Hudlicky, Organic Reaction 35 (1988) 513–637.
[12] P.A. Messina, K.C. Mange, W.J. Middleton, Journal of Fluorine Chemistry 42 (1989) 137–143.
[13] R. Surmont, G. Verniest, A. De Groot, J.W. Thuring, N. De Kimpe, Advanced Synthesis and Catalysis 352 (2010) 2751–2756.
[14] R. Surmont, G. Verniest, A. De Weweire, J.W. Thuring, G. Macdonald, F. Deroose, N. De Kimpe, Synlett 12 (2009) 1933–1936.
[15] L. Lunazzi, D. Casarini, M.A. Cremonini, Tetrahedron 47 (1991) 7465–7470, and references therein.
[16] V.G. Pashinnik, E.G. Martyniuk, M.R. Tabachuk, YuG. Shermolovich, L.M. Yagupolskii, Synthetic Communications 33 (2003) 2505–2509.
[17] H.G. Schnöckel, H. Willner, in: B. Schrader (Ed.), Infrared and Raman Spectroscopy, Methods and Applications, VCH, Weinheim, 1994.
[18] For example, see:
(a) X.Q. Zeng, H. Beckers, E. Bernhardt, H. Willner, Inorganic Chemistry 50 (2011) 8679–8684;
(b) X.Q. Zeng, M. Gerken, H. Beckers, H. Willner, Inorganic Chemistry 49 (2010) 9694–9699;
(c) X.Q. Zeng, M. Gerken, H. Beckers, H. Willner, Inorganic Chemistry 49 (2010) 3002–3010.
[19] CrysAlisPro, version 1.171.33.42, Oxford Diffraction Ltd., Oxford, U.K., 2010.
[20] L.J. Farrugia, WinGX v1.64.05—An Integrated System of Windows Programs for the Solution, Refinement and Analysis of Single Crystal X-ray Diffraction Data, University Glasgow, Glasgow, Scotland, 2003 (J. Appl. Crystallogr. 32 (1999) 837–838).
[21] G.M. Sheldrick, SHELXS-97, Program for Crystal Structure Solution; Universität Göttingen, Göttingen, Germany, 1997.
[22] K. Brandenburg, Diamond, Version.2.1e; Crystal Impact GbR, Bonn, Germany, 2001.
[23] M.J. Frisch, G.W. Trucks, H.B. Schlegel, G.E. Scuseria, M.A. Robb, J.R. Cheeseman, J.A. Montgomery Jr., T. Vreven, K.N. Kudin, J.C. Burant, et al., Gaussian 03, Revision D.01, Gaussian, Inc., Wallingford, CT, 2003.
[24] A.D. Becke, Journal of Chemical Physics 98 (1993) 5648–5652.
[25] (a) M. Head-Gordon, J.A. Pople, M.J. Frisch, Chemical Physics Letters 153 (1988) 503–506;
(b) S. Saebø, J. Almlöf, Chemical Physics Letters 154 (1989) 83–89;
(c) M.J. Frisch, M. Head-Gordon, J.A. Pople, Chemical Physics Letters 166 (1990) 275–280;
(d) M.J. Frisch, M. Head-Gordon, J.A. Pople, Chemical Physics Letters 166 (1990) 281–289;
(e) M. Head-Gordon, T. Head-Gordon, Chemical Physics Letters 220 (1994) 122–128.
[26] A.E. Reed, L.A. Curtis, F. Weinhold, Chemical Reviews 88 (1988) 899–926.
[27] A.J. Barnes, W.J. Orville-Thomas, A. Müller, R. Gaufres (Eds.), Nato Advanced Study Institutes Series C, vol. 76. Matrix Isolation Spectroscopy, D. Reidel Publishing Company, Dortrecht, 1981, pp. 531.
[28] A.A. El-Binary, P. Klaeboe, C.J. Nielsen, Journal of Molecular Structure 218 (1990) 73–80.
[29] M. Bodenbinder, S.E. Ulic, H. Willner, Journal of Physical Chemistry 98 (1994) 6441–6444.